ECCOMAS Congress 2016
VII European Congress on Computational Methods in Applied Sciences and Engineering
M. Papadrakakis, V. Papadopoulos, G. Stefanou, V. Plevris (eds.)
Crete Island, Greece, 5–10 June 2016

FINITE ELEMENT METAMODELING OF UNCERTAIN STRUCTURES

Vasilis K. Dertimanis[1], Dimitrios Giagopoulos[2], and Eleni N. Chatzi[1]

[1] ETH Zurich, Inst. of Structural Engineering, Department Of Civil, Environmental and Geomatic Engineering
Stefano-Franscini-Platz 5, 8093 Zurich, Switzerland
e-mail: {v.derti,chatzi}@ibk.baug.ethz.ch

[2] University of Western Macedonia, Department of Mechanical Engineering
Bakola & Sialvera Str., 501 00 Kozani, Greece
e-mail: dgiagopoulos@uowm.gr

Keywords: Substructuring, Metamodeling, Vehicle dynamics, Finite elements, Model reduction, Polynomial chaos, B–splines, ARX.

Abstract. *The necessity for more detailed descriptions of both structural geometry and mechanical properties, renders the use of highly detailed finite element (FE) models almost prohibitive for complex, large structures. This becomes even more challenging when taking into account that structural systems and their excitations are often characterized by parameter uncertainty. To this end, this study addresses the problem of estimating reduced order metamodels for the accurate representation of computationally costly numerical models. A substructuring approach is adopted for segregating the modeled system into a series of smaller components, by separating the parts with exclusively linear characteristics from the uncertain ones. Each of these components is then approximated by corresponding ARX representations, the parameters of which are functionally dependent on uncertain input parameters, also accounting for uncertainty propagation through the FE model. These functional models are coupled in the time domain to formulate a complete metamodel of the system. The effectiveness of the proposed method is illustrated through its application on the metamodeling of a vehicle frame with uncertain suspension. The results demonstrate the efficiency of the proposed methodology for accurate prediction and simulation of the numerical model dynamics.*

1 INTRODUCTION

FE modeling has nowadays become a standard tool for the numerical simulation of civil, mechanical and aeronautical engineering structures [1, 2, 3] and is extensively used for design optimization [4], reliability analysis [5, 6], as well as for the simulation of hysteretic behaviour [7, 8] and damage [9, 10]. When dynamic loading is involved, however, the increased complexity of FE models renders the efficient characterization of the structural response a quite difficult task, especially for large structures, despite the rapidly growing computational power and the continuous development of increasingly efficient algorithms [11, 12]. A common strategy in such cases is to apply less refined macro-models to the simulation of the global behaviour using, for example, model reduction methods [13], and then implement more detailed local FE micro-models for the description of complex parts of the structure.

Alternatively, substructuring techniques [14] can be considered, under which the total structure is disassembled into several subcomponents that can be analysed separately. This framework retains many advantages over other approaches, since it allows isolation of areas, in which more detail is required, it can be successfully implemented in parallel computing and software–in–the–loop schemes, while it allows for flexible usage of the subcomponents in other structures. This latter advantage is one of the most significant aspects of substructuring, taking under consideration modern challenges of production engineering [15], where coupling of numerical models with fabricated subcomponents (e.g., in the form of experimental prototypes [16]) is a common practice, using hybrid testing and hardware–in–the–loop methods [17].

Another important aspect that must be taken into consideration during the simulation process corresponds to the inherent uncertainty that characterizes critical parameters of the available FE model, such as its associated mechanical properties, the range of operational and environmental conditions under which the structure is designed to operate and, of course, the diverse nature and levels of all possible excitations. In dealing with this issue, Monte Carlo–based methods have been widely applied, despite the necessity for a large number of simulations, with each one demanding excessive computational cost. In contrast to these, simpler representations of the numerical model are formulated using metamodelling techniques, which essentially build a parametric model of the original FE one, termed as *metamodel* or *surrogate model* [18, 19]. This metamodel must be able to predict the dynamic response in a computationally inexpensive way and with sufficient accuracy [20, 21].

Under this perspective, the problem faced in the current study pertains to the determination of the structural response in critical points of the structure using a *small number* of *computationally inexpensive* simulations, which take into account the whole operational range of inherent uncertainties and provide a representative behavioral map of the structure. A special case to this problem corresponds to the availability of physically available parts of the structure, for which experimental data, rather than an analytical model, are available. To address this problem, a process that consists of three overlapping and interrelated stages, namely, (i) the *substructuring* stage, (ii) the *model reduction* stage and (iii) the *metamodeling* stage, is proposed and outlined in the following.

The paper is organized as follows: Section 2 outlines the proposed methodology and describes the associated substructuring, model reduction and metamodeling stages. Section 3 contains a numerical study pertaining to a "vehicle"–like prototype that consists of a frame substructure and one linear suspension with uncertain stiffness. Finally, in Section 4 the results are summarized and remarks for further research are given.

2 THE PROPOSED FRAMEWORK

2.1 Problem formulation

Let us consider an n–DOF FE model of a damped structural system that can be mathematically represented by a second–order vector differential equation of the form

$$\mathbf{M}(\boldsymbol{\xi})\ddot{\mathbf{q}}(t) + \mathbf{D}(\boldsymbol{\xi})\dot{\mathbf{q}}(t) + \mathbf{K}(\boldsymbol{\xi})\mathbf{q}(t) = \mathbf{f}(t) \tag{1}$$

where $\mathbf{M}(\boldsymbol{\xi})$, $\mathbf{D}(\boldsymbol{\xi})$ and $\mathbf{K}(\boldsymbol{\xi})$ are the real $[n \times n]$ mass, viscous damping and stiffness matrices, $\mathbf{q}(t)$ is the $[n \times 1]$ vibration displacement vector and $\mathbf{f}(t)$ is the $[n \times 1]$ vector of excitations.

The dependence of the structural matrices to $\boldsymbol{\xi}$ is herein used to notate their variability due to a number of uncertain parameters related with either inherent properties of the structure, or exogenous random variables, e.g. geometry, mass distribution, environmental conditions and so on. For a number of L such uncertain parameters it follows that $\boldsymbol{\xi}(t) = [\xi_1, \xi_2, \ldots, \xi_L]$. In its most general statistical representation, the parameter vector $\boldsymbol{\xi}$ may be considered as a realization of the vector random process $\boldsymbol{\Xi}$ with joint PDF $f_{\boldsymbol{\Xi}}(\boldsymbol{\xi})$. Simpler realizations are possible if it is assumed that each parameter ξ_k is a realization of an independent random process Ξ_k with PDF $f_{\Xi_k}(\xi_k)$.

In this setting, the problem addressed herein aims at simulating the structural response, in the form of vibration displacement, velocity, or acceleration, under the following conditions:

- The size n of the FE model of the structure is prohibitely large for computationally efficient direct simulation.
- The structure can be split into a number of smaller substructures and all the associated boundaries can be adequately described.
- A statistical description of the uncertain parameters and the excitations is available for the whole operating range of the structure.

2.2 Substructuring

Assume that the total structure, described by Eq. 1, is constructed by the proper assembly of two substructures, $A(\boldsymbol{\xi})$ and $B(\boldsymbol{\xi})$. Then, instead of attempting to simulate the whole structure, it is possible to carry out distributed simulations for each substructure, provided that the common interface among the subdomains is appropriately defined. Indeed, the equations of motion that describe each substructure are

$$\mathbf{M}_A(\boldsymbol{\xi})\ddot{\mathbf{q}}_A(t) + \mathbf{D}_A(\boldsymbol{\xi})\dot{\mathbf{q}}_A(t) + \mathbf{K}_A(\boldsymbol{\xi})\mathbf{q}_A(t) = \mathbf{f}_A(t) + \mathbf{h}_A(t) \tag{2}$$

and

$$\mathbf{M}_B(\boldsymbol{\xi})\ddot{\mathbf{q}}_B(t) + \mathbf{D}_B(\boldsymbol{\xi})\dot{\mathbf{q}}_B(t) + \mathbf{K}_B(\boldsymbol{\xi})\mathbf{q}_B(t) = \mathbf{f}_B(t) + \mathbf{h}_B(t) \tag{3}$$

with all the associated quantities previously defined, with the exception of $\mathbf{h}_*(t)$, which corresponds to the vector of connecting forces. Then, from de Klerk *et al.* [14], recovery of Eq. 1 proceeds by first stacking the substructures as

$$\underbrace{\begin{bmatrix}\mathbf{M}_A & \mathbf{O}\\ \mathbf{O} & \mathbf{M}_B\end{bmatrix}}_{\overline{\mathbf{M}}}\begin{bmatrix}\ddot{\mathbf{q}}_A(t)\\ \ddot{\mathbf{q}}_B(t)\end{bmatrix} + \underbrace{\begin{bmatrix}\mathbf{D}_A & \mathbf{O}\\ \mathbf{O} & \mathbf{D}_B\end{bmatrix}}_{\overline{\mathbf{D}}}\begin{bmatrix}\dot{\mathbf{q}}_A(t)\\ \dot{\mathbf{q}}_B(t)\end{bmatrix} + \underbrace{\begin{bmatrix}\mathbf{K}_A & \mathbf{O}\\ \mathbf{O} & \mathbf{K}_B\end{bmatrix}}_{\overline{\mathbf{K}}}\underbrace{\begin{bmatrix}\mathbf{q}_A(t)\\ \mathbf{q}_B(t)\end{bmatrix}}_{\overline{\mathbf{q}}(t)} = \underbrace{\begin{bmatrix}\mathbf{f}_A(t)\\ \mathbf{f}_B(t)\end{bmatrix}}_{\overline{\mathbf{f}}(t)} + \underbrace{\begin{bmatrix}\mathbf{h}_A(t)\\ \mathbf{h}_B(t)\end{bmatrix}}_{\overline{\mathbf{h}}(t)} \tag{4}$$

and then by specifying the compatibility (identical displacements of the coupled DOFs) and equilibrium (action–reaction forces) conditions as,

$$\mathbf{C}\overline{\mathbf{q}}(t) = \mathbf{0} \quad \text{and} \quad \mathbf{E}^T\overline{\mathbf{h}}(t) = \mathbf{0} \tag{5}$$

respectively, with $\mathbf{C}$ and $\mathbf{E}$ denoting signed Boolean and Boolean matrices, respectively. Accordingly, by defining a unique set of structural DOFs, $\mathbf{q}(t)$, through

$$\overline{\mathbf{q}}(t) = \mathbf{E}\mathbf{q}(t) \tag{6}$$

it follows from Eq. 5 that $\mathbf{C}\overline{\mathbf{q}}(t) = \mathbf{C}\mathbf{E}\mathbf{q}(t) = \mathbf{0}$, from which $\mathbf{E} = \text{null}\{\mathbf{C}\}$. Substituting Eq. 6 to Eq. 4 implies

$$\overline{\mathbf{M}}\mathbf{E}\ddot{\mathbf{q}}(t) + \overline{\mathbf{D}}\mathbf{E}\dot{\mathbf{q}}(t) + \overline{\mathbf{K}}\mathbf{E}\mathbf{q}(t) = \overline{\mathbf{f}}(t) + \overline{\mathbf{h}}(t) \tag{7}$$

thus, multiplication by $\mathbf{E}^T$ leads to the representation of the total structure by Eq. 1 with

$$\mathbf{M} = \mathbf{E}^T\overline{\mathbf{M}}\mathbf{E}, \;\; \mathbf{D} = \mathbf{E}^T\overline{\mathbf{D}}\mathbf{E}, \;\; \mathbf{K} = \mathbf{E}^T\overline{\mathbf{K}}\mathbf{E}, \;\; \mathbf{f}(t) = \mathbf{E}^T\overline{\mathbf{f}}(t) \tag{8}$$

2.3 Model reduction

When the substructures still retain a large number of DOFs, model reduction can be used to further suppress the DOFs. While several other alternatives are possible (the interested reader is referred to Antoulas [13] for an authoritative treatment) the Ritz transformation is currently implemented. Following the previous discussion and if only the substructure $A(\boldsymbol{\xi})$ requires reduction, a new set of coordinates is provided by

$$\mathbf{q}_A(t) = \boldsymbol{\Psi}_A\mathbf{q}_{AR}(t) \tag{9}$$

where $\boldsymbol{\Psi}_A$ is a subset of the normal modes of Eq. 2, the selection of which depends on the frequency range examined. Applying this transformation to Eq. 2 and pre–multiplying by $\boldsymbol{\Psi}_A^T$ implies

$$\mathbf{M}_{AR}(\boldsymbol{\xi})\ddot{\mathbf{q}}_{AR}(t) + \mathbf{D}_{AR}(\boldsymbol{\xi})\dot{\mathbf{q}}_{AR}(t) + \mathbf{K}_{AR}(\boldsymbol{\xi})\mathbf{q}_{AR}(t) = \mathbf{f}_{AR}(t) + \mathbf{h}_{AR}(t) \tag{10}$$

for

$$\begin{aligned} \mathbf{M}_{AR} = \boldsymbol{\Psi}^T\mathbf{M}_A\boldsymbol{\Psi}, \;\; \mathbf{D}_{AR} = \boldsymbol{\Psi}^T\mathbf{D}_A\boldsymbol{\Psi}, \;\; \mathbf{K}_{AR} = \boldsymbol{\Psi}^T\mathbf{K}_A\boldsymbol{\Psi} \\ \mathbf{f}_{AR}(t) = \boldsymbol{\Psi}^T\mathbf{f}_A(t), \;\; \mathbf{h}_{AR}(t) = \boldsymbol{\Psi}^T\mathbf{h}_A(t) \end{aligned} \tag{11}$$

and corresponds to a reduced representation of the substructure $A(\boldsymbol{\xi})$.

2.4 Metamodeling

The third stage of the proposed methodology aims at estimating a reduced model of Eq. 3. Consider the case where the substructure $B(\boldsymbol{\xi})$ contains one DOF, a single excitation and a single uncertain parameter, so that Eq. 3 corresponds to a scalar nonlinear differential equation and $\boldsymbol{\xi} = \xi$. Then the structural output can be approximated using Adaptable Functional Series Autoregressive with eXogenous input (AFS-ARX) models of the form [22]

$$y[t,\xi] + \sum_{i=1}^{na}\alpha_i(\xi)y[t-i] = \sum_{i=0}^{nb}\beta_i(\xi)u[t-i] + e[t] \tag{12}$$

where $y[t]$ and $u[t]$ denote the model's output and input, respectively, $\alpha_i(\xi)$ and $\beta_i(\xi)$ are the coefficients of the AR and exogenous polynomials, of orders na and nb, respectively, and $e[t] \sim \mathcal{N}(0, \sigma_e^2)$ is the model's zero-mean Gaussian residual sequence.

The AFS-ARX(na, nb) model of Eq. 12 accounts for the uncertainty of $B(\boldsymbol{\xi})$ through the regression parameters $\theta_i(\xi)$, which are currently admitting a representation based on B–spline functions

$$\alpha_i(\xi) = \sum_{j=1}^{p} \alpha_{ij} S_{j,k}(\xi, \boldsymbol{\delta}_\alpha) \tag{13a}$$

$$\beta_i(\xi) = \sum_{j=1}^{p} \beta_{ij} S_{j,k}(\xi, \boldsymbol{\delta}_\beta) \tag{13b}$$

with $S_{j,k}(\xi, \boldsymbol{\delta})$ denoting the sequence of B-splines of order k and of functional subspace parameter vector $\boldsymbol{\delta} \equiv [\tau_{k+1}, \dots, \tau_p]^T$, henceforth referred to as the vector of free knots, of dimension $\dim(\boldsymbol{\delta}) = p - k$, consisting of the non-decreasing sequence of the free internal knots. Given a realization ξ, a particularly convenient way for defining $S_{j,k}(\xi, \boldsymbol{\delta})$ is obtained by means of the Cox-de Boor recursion formula for the normalized B-splines [23, p. 90], according to which

$$S_{j,1}(\xi, \boldsymbol{\delta}) = \begin{cases} 1 & \text{if } \tau_j \leq \xi < \tau_{j+1} \\ 0 & \text{otherwise} \end{cases} \tag{14a}$$

$$S_{j,i}(\xi, \boldsymbol{\delta}) = w_{j,i}(\xi) S_{j,i-1}(\xi, \boldsymbol{\delta}) + (1 - w_{j,i}(\xi)) S_{j+1,i-1}(\xi, \boldsymbol{\delta}), \quad \text{for } 1 < i \leq k \tag{14b}$$

where

$$w_{j,i}(\xi) = \begin{cases} \frac{\xi - \tau_j}{\tau_{j+i-1} - \tau_j} & \text{if } \tau_j < \tau_{j+i-1}, \\ 0 & \text{otherwise.} \end{cases} \tag{14c}$$

It is noted that since the internal free knots form a non decreasing sequence of real numbers, they have to satisfy proper constraints in relation to their bounds and order [24].

The efficient representation of $B(\xi)$ through AFS-ARX(na, nb) models is succeeded through the establishment and the solution of an associated identification problem, in which all the unknown parameters of the model are estimated, that is, the integers na, nb, p and k, the parameters α_{ij} and β_{ij} in Eq. 13, the vectors of free knots $\boldsymbol{\delta}_\alpha$ and $\boldsymbol{\delta}_\beta$, as well as the residual variance σ_e^2. To this end, the original AFS-ARX(na, nb) model of Eq. 12 is transformed into a linear regression form as

$$y[t] = \boldsymbol{\phi}[t, \boldsymbol{\delta}]\boldsymbol{\theta} + e[t] \tag{15}$$

for $\boldsymbol{\delta} = [\boldsymbol{\delta}_\alpha \;\; \boldsymbol{\delta}_\beta]^T$ and

$$\boldsymbol{\phi}[t, \boldsymbol{\delta}] = \big[-y[t-1] S_{1,k}(\xi, \boldsymbol{\delta}_\alpha) \;\; -y[t-1] S_{2,k}(\xi, \boldsymbol{\delta}_\alpha) \;\; \dots \;\; x[t-nb] S_{p,k}(\xi, \boldsymbol{\delta}_\beta) \big] \tag{16}$$

and

$$\boldsymbol{\theta} = [\alpha_{1,1} \; \alpha_{1,2} \; \dots \; \alpha_{na,p}]^T \tag{17}$$

If input–output data are available over $t = 1, \dots, N$ then Eq. 15 yields

$$\mathbf{y} = \boldsymbol{\phi}(\boldsymbol{\delta})\boldsymbol{\theta} + \mathbf{e} \tag{18}$$

where $\mathbf{y} = [y[1] \ \dots \ y[N]]^T$, $\boldsymbol{\phi}(\boldsymbol{\delta}) = [\boldsymbol{\phi}[1,\boldsymbol{\delta}] \ \dots \ \boldsymbol{\phi}[N,\boldsymbol{\delta}]]^T$ and $\mathbf{y} = [e[1] \ \dots \ e[N]]^T$. Notice that the AFS-ARX(na, nb) model must include all available statistical information of ξ. Thus, a number of simulations (or experiments, if the substructure $B(\xi)$ is experimental) is performed, say L, given a set of uncertainty parameter realizations, ξ_l, and the corresponding input–output data sets are obtained, $\mathbf{x}_l = [x_l[1] \ \dots \ x_l[N]]^T$ and $\mathbf{y}_l = [y_l[1] \ \dots \ y_l[N]]^T$, respectively, for $l = 1, 2, \dots, L$. Each one of these sets must satisfy Eq. 18, so that

$$\mathbf{y}_l = \boldsymbol{\phi}_l(\boldsymbol{\delta})\boldsymbol{\theta} + \mathbf{e}_l \tag{19}$$

By pooling Eq. 19 for all available experiments it follows that

$$\begin{bmatrix} \mathbf{y}_1 \\ \vdots \\ \mathbf{y}_l \end{bmatrix} = \begin{bmatrix} \boldsymbol{\phi}_1(\boldsymbol{\delta}) \\ \vdots \\ \boldsymbol{\phi}_l(\boldsymbol{\delta}) \end{bmatrix} \theta + \begin{bmatrix} \mathbf{e}_1 \\ \vdots \\ \mathbf{e}_l \end{bmatrix} \Rightarrow \mathbf{Y} = \boldsymbol{\Phi}(\boldsymbol{\delta})\boldsymbol{\theta} + \mathbf{E} \tag{20}$$

and the parameter vector $\boldsymbol{\theta}$ can be recovered by the least squares estimate

$$\boldsymbol{\theta} = \Big[\boldsymbol{\Phi}(\boldsymbol{\delta})^T\boldsymbol{\Phi}(\boldsymbol{\delta})\Big]^{-1}\boldsymbol{\Phi}(\boldsymbol{\delta})^T\mathbf{Y} = \boldsymbol{\Phi}(\boldsymbol{\delta})^\dagger\mathbf{Y} \tag{21}$$

with $\boldsymbol{\Phi}(\boldsymbol{\delta})^\dagger$ denoting the pseudo-inverse of $\boldsymbol{\Phi}(\boldsymbol{\delta})$. Since the parameter vector $\boldsymbol{\theta}$ depends on the vector of free knots $\boldsymbol{\delta}$, the latter must be estimated prior to the implementation of Eq. 21. Notice that the prediction error sequence $\mathbf{E}$ can be expressed as

$$\begin{aligned} \mathbf{E} &= \mathbf{Y} - \boldsymbol{\Phi}(\boldsymbol{\delta})\boldsymbol{\theta} \Rightarrow \\ &= \mathbf{Y} - \boldsymbol{\Phi}(\boldsymbol{\delta})\boldsymbol{\Phi}(\boldsymbol{\delta})^\dagger\mathbf{Y} \Rightarrow \\ &= \Big[\mathbf{I} - \boldsymbol{\Phi}(\boldsymbol{\delta})\boldsymbol{\Phi}(\boldsymbol{\delta})^\dagger\Big]\mathbf{Y} \end{aligned} \tag{22}$$

Thus, $\boldsymbol{\delta}$ can be estimated by the solution of the following nonlinear optimization problem [24]

$$\hat{\boldsymbol{\delta}} = \arg\min_{\boldsymbol{\delta}} V_{\text{VP}}(\boldsymbol{\delta}) \doteq \arg\min_{\boldsymbol{\delta}} \|(\mathbf{I} - \boldsymbol{\Phi}(\boldsymbol{\delta})\boldsymbol{\Phi}(\boldsymbol{\delta})^\dagger)\mathbf{Y}\|^2 \tag{23}$$

A final note in metamodeling refers to the cases of large data: observe that from Eqs. 18–20 the involved matrices, $\mathbf{Y}$ and $\boldsymbol{\Phi}(\boldsymbol{\delta})$, can become quite large even for small values of na, nb, p, L and N. Indicatively, for an AFS-ARX(2,3) model with B–spline basis of second order, $p = 3$, $L = 20$ and $N = 500$, their sizes are $[10000 \times 1]$ and $[10000 \times 15]$, respectively. In such cases, and in order to avoid numerical inconsistencies, it may be preferable to model directly the parameters $\alpha_i(\xi)$ and $\beta_i(\xi)$ from Eq. 13, in a process that can be easily realized in parallel. Such an estimation problem turns out to be a typical data–driven uncertainty quantification one that can be solved using, for example, the method described in Spiridonakos *et al.* [24]. This alternative is adopted for the analysis presented in the next section.

3 IMPLEMENTATION

The method's performance and effectiveness is assessed via the metamodeling of a "vehicle"–like prototype that consists of a frame substructure, displayed in Fig. 1, which is connected to four wheelsets through corresponding primary linear suspensions. Each wheelset is modeled as a mass with one degree of freedom and with equivalent stiffness and damping, while all suspensions are identical, except from the front right one that is characterized by uncertain stiffness. The associated parameters of the model are displayed in Tab. 1.

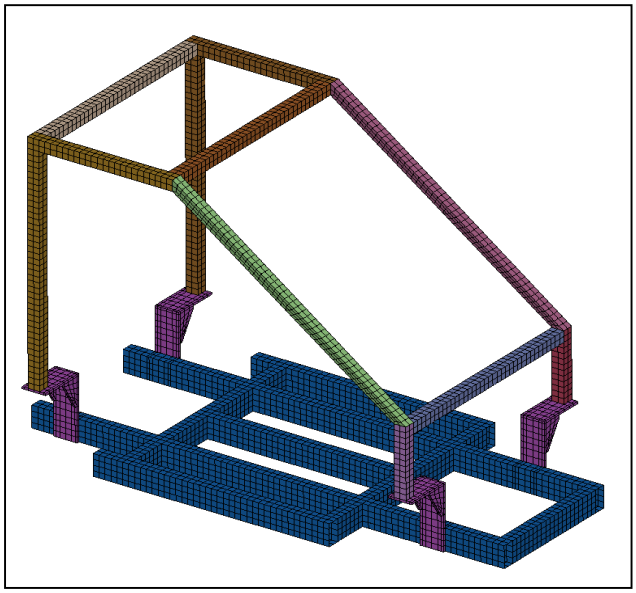

Figure 1: The frame substructure.

Quantity	**Symbol**	**Value**	**Unit**
Frame material density	E	2.1×10^{11}	N/m
Frame material modulus	ρ	7850	kg/m^3
Wheelset mass	m_w	16	kg
Wheelset stiffness	k_w	35	N/m
Wheelset damping	c_w	0	Ns/m
Suspension stiffness	k_s	22	N/m
Suspension damping	c_s	5	Ns/m
Uncertain stiffness	k_{fr}	$\sim \mathcal{N}(22, 6)$	N/m
Road profile	r_{fr}	$\sim \mathcal{N}(0, 7 \times 10^{-3})$	m

Table 1: Parameters of the simulated vehicle.

The FE model of the frame is constructed using quadrilateral shell and hexahedral solid elements, resulting in 45564 DOFs. Model reduction is accordingly applied using the method outlined in Section 2.3, leading to a reduced model of only 54 DOFs. The latter is then connected to the wheelset–suspension subsystems and the total structure is simulated by assuming excitation only in the front right position, which consists of a zero mean Gaussian process that is filtered using a 10th order digital Butterworth filter with low-pass frequency at 30 Hz. A number of $L = 50$ simulations is performed at a sampling period $T_s = 1$ ms and for $t = 5$ s, each one under a specific realization of k_{fr}, drawn using the latin hypercube sampling (LHS) method and illustrated in Fig. 2. The substructure $B(\xi)$ is herein selected to be the subsystem that has the road-induced force applied to the wheelset mass as an input and the vertical acceleration of the common boundary between the frame and the front right suspension as an output. Vibration excitation-response pairs of $N = 5000$ data are thus stored after every simulation. Figure 3 displays an indicative data pair that corresponds to $L = 20$.

To examine the consistency of the method under the availability of limited simulations and /or data, estimation of $B(\xi)$ is conducted using only simulations $\#$ 16 until $\#$ 30 (see Fig. 2). In

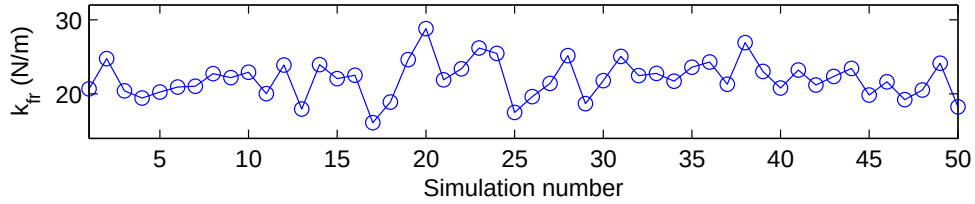

Figure 2: The uncertain stiffness k_{fr} for the 50 simulations conducted.

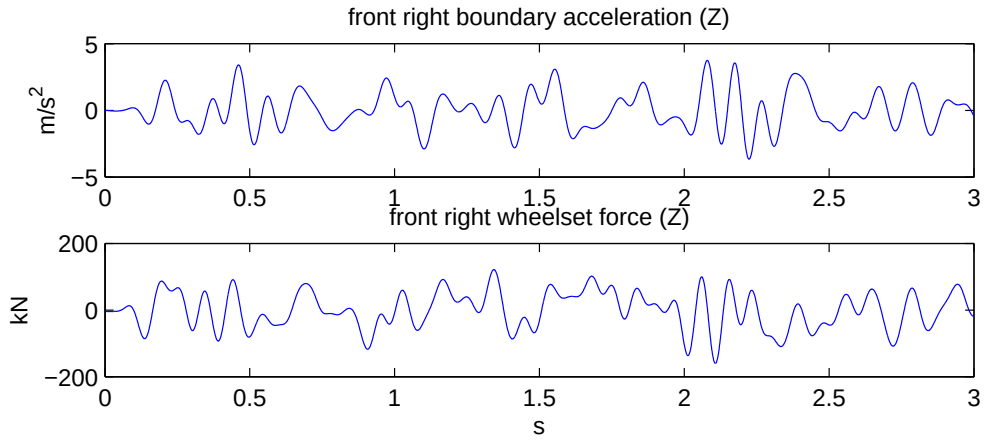

Figure 3: Vibration acceleration response at the front right boundary and road induced force for $L = 20$.

every case, the first 2000 values are extracted from the input–output data set, in order to avoid modeling transient effects, and the set used for identification consists of only the next 1000 data. In order to get an initial insight some initial trial-and-error modeling attempts were performed, revealing that AFS-ARX(2,3) are potentially adequate for representing the substructure $B(\xi)$. This results in five parameters, α_1, α_2, β_0, β_1 and β_2, which must be expressed in respect to the uncertain stiffness. A two–stage procedure is utilized to this purpose:

[S1] Simple ARX(2,3) models are estimated for every simulation and five new (compressed) data sets are formulated, with the uncertain stiffness as input and the AR/X parameter as output.

[S2] Models in the form of Eq. 13 are fitted to each parameter, for $p = 1, \ldots, 10$ and $k = 1, \ldots, 4$.

Figure 4 illustrates the results of this procedure. All examined models returned almost perfect match, as can be seen by the percentage fitness to the data, calculated by

$$\text{fit} = 100\left(1 - \frac{\|q - \hat{q}\|}{\|q - \bar{q}\|}\right)\ (\%) \tag{24}$$

where q and $\hat{q}$ denote true and estimated quantity, respectively, and $\bar{q}$ denotes mean value, with only $S_{j,1}$ exhibiting slightly lower performance. Thus, a model with B-spline basis functions of second order, $S_{j,2}$, and of $p = 3$ was selected for the uncertainty quantification of the AFS-ARX(3,2) parameters. For this model, Fig. 4 further displays the true (e.g., the ones estimated during step **[S1]** above) parameter values versus the model calculated ones.

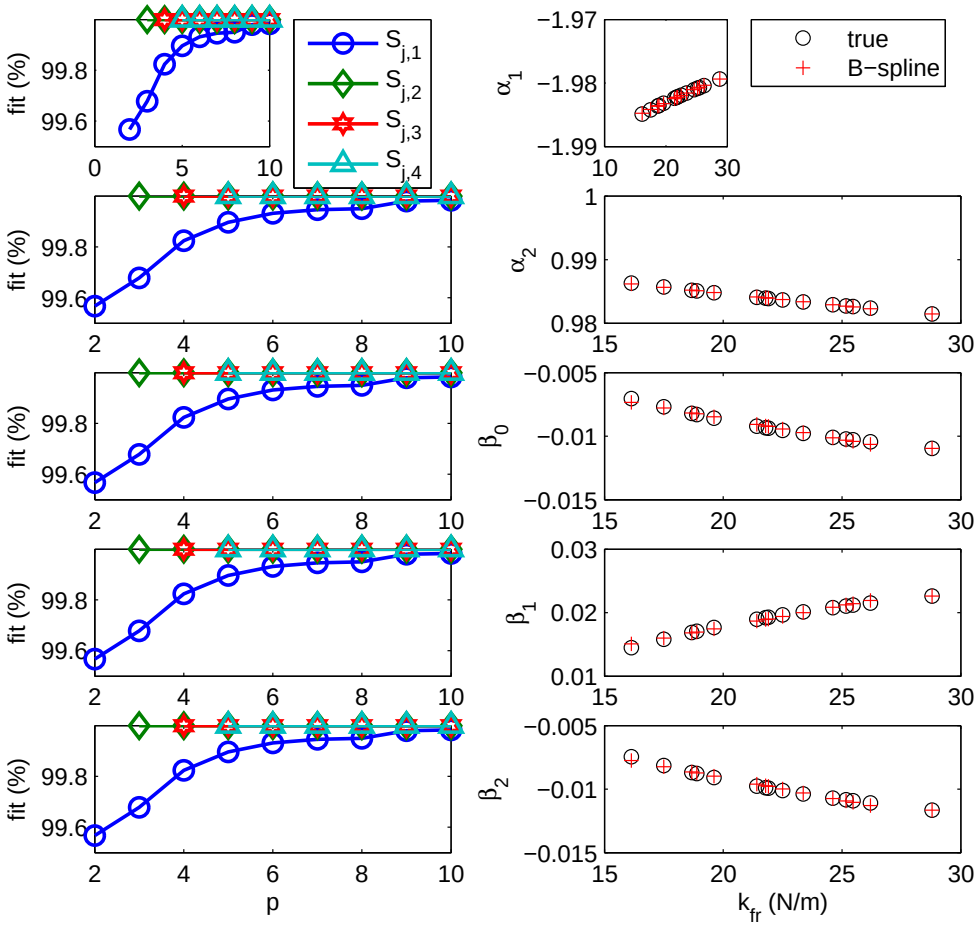

Figure 4: Results of the uncertainty quantification process for each parameter of the AFS-ARX(2,3) model. Left side: percentage fitness to data of every estimated model. Right side: true versus model-based outputs, using Eq. 13 with $p = 3$ and $k = 2$.

The identified AFS-ARX(3,2) model is finally validated against its applicability to the whole spectrum of possible uncertain values. To this end, the data from four simulations that were not used in the estimation process (randomly selected, with two realizations among $\#1, \ldots, \#15$ and two among $\#31, \ldots, \#50$) are forwarded into the model and the predicted output is plotted over the one simulated from the total structure in Fig. 5. Excellent matching is confirmed, implying that the AFS-ARX(3,2) model can adequately replace substructure $B(\xi)$.

4 CONCLUSION

A process for the effective simulation of large–scale, uncertain FE models was outlined in this study, consisting of three interrelated stages that take on the substructuring, the model reduction and the metamodeling steps. The illustrated results provide significant indication of effectiveness and suggest further investigation in this path, with respect to a number of issues that remain active challenges in the field of structural modeling and simulation. Automation of the proposed process, by focusing on the smart interpretation of boundary constraints, the extension to simultaneous substructuring and metamodeling of nonlinear models, as well as the implementation to real-time hybrid testing techniques are issues that are currently being investigated by the authors.

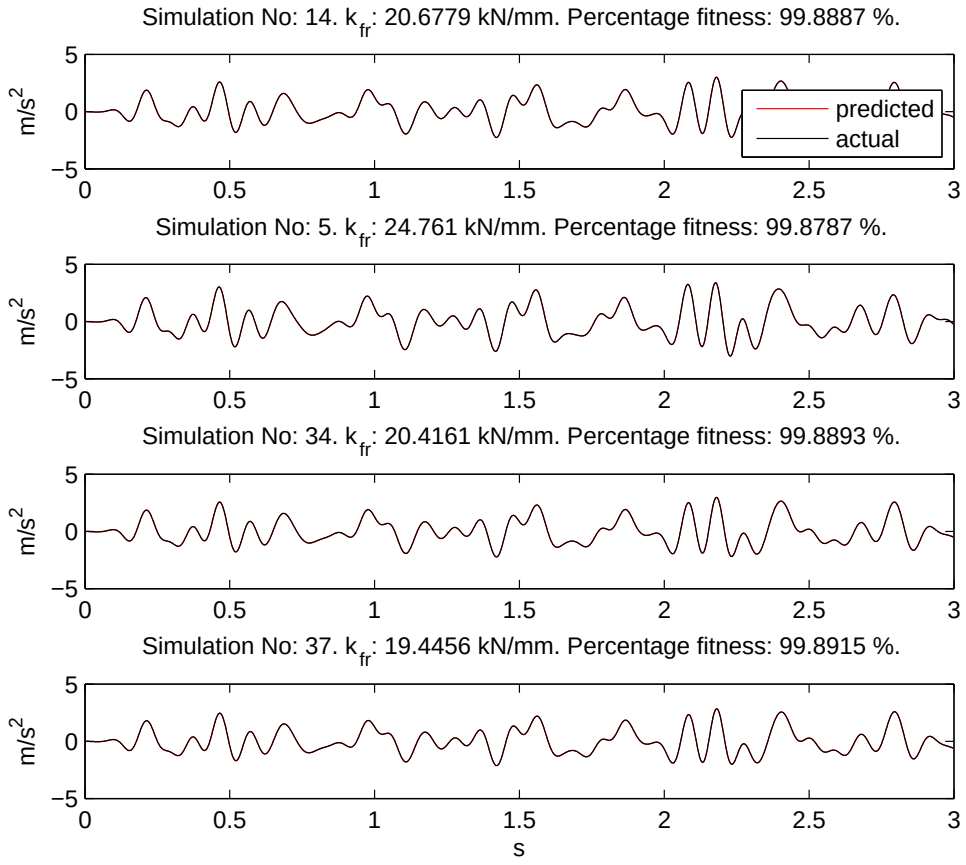

Figure 5: Validation of the AFS-ARX(2,3) model in for simulations not used for identification.

REFERENCES

[1] J. Argyris and S. Kelsey. Energy theorems and structural analysis. *Aircraft Engineering*, 26-27, 1954-1955.

[2] K.-J. Bathe. Finite element method. In B. Wah, editor, *Wiley Encyclopedia of Computer Science and Engineering*, pages 1253–1264. Wiley & Sons, Inc., 2009.

[3] R. Clough. The finite element method in plane stress analysis. In *2nd ASCE Conference on Electronic Computation, Pittsburgh, PA, USA, 1960 September 8-9*, pages 345–378, 1960.

[4] P. Chang and J. Perl. A finite element based approach to multi-objective structural optimization using goal programming. *Engineering Optimization*, 13(1):65–82, 1988.

[5] Armen Der Kiureghian and Jyh-Bin Ke. The stochastic finite element method in structural reliability. *Probabilistic Engineering Mechanics*, 3(2):83–91, 1988.

[6] Dian-Qing Li, Te Xiao, Zi-Jun Cao, Chuang-Bing Zhou, and Li-Min Zhang. Enhancement of random finite element method in reliability analysis and risk assessment of soil slopes using subset simulation. *Landslides*, pages 1–11, 2015.

[7] F. Taucer, E. Spacone, and F. Filippou. A fiber beam-column element for seismic response analysis of reinforced concrete structures. Technical Report UCB/EERC 91/17, Earthquake Engineering Research Center, Univ. of California, Berkeley, 1992.

[8] S. Triantafyllou and V. Koumousis. Bouc-wen type hysteretic plane stress element. *Journal of Engineering Mechanics*, 138(3):235–246, 2012.

[9] D. Rabinovich, D. Givoli, and S. Vigdergauz. Xfem-based crack detection scheme using a genetic algorithm. *International Journal for Numerical Methods in Engineering*, 71(9):1051–1080, 2007.

[10] H. Waisman, E. Chatzi, and S. Smyth. Detection and quantification of flaws in structures by the extended finite element method and genetic algorithms. *International Journal for Numerical Methods in Engineering*, 82(3):303–328, 2010.

[11] L. Pichler, A. Gallina, T. Uhl, and L.A. Bergman. A meta-modeling technique for the natural frequencies based on the approximation of the characteristic polynomial. *Computers and Structures*, 102-103:108–116, July 2012.

[12] S. Gholizadeh and E. Salajegheh. Optimal design of structures subjected to time history loading by swarm intelligence and an advanced metamodel. *Computer Methods in Applied Mechanics and Engineering*, 198:2936–2949, 2009.

[13] A.C. Antoulas. *Approximation of Large-Scale Dynamical Systems*. Society for Industrial and Applied Mathematics, Philadelphia, USA, 2005.

[14] D. de Klerk, D.J. Rixen, and S.N. Voormeeren. General framework for dynamic substructuring: History, review, and classification of techniques. *AIAA Journal*, 46(5):1169–1181, 2008.

[15] H. Van Der Auweraer, J. Anthonis, S. De Bruyne, and J. Leuridan. Virtual engineering at work: The challenges for designing mechatronic products. *Engineering with Computers*, 29(3):389–408, 2013.

[16] D. Giagopulos and S. Natsiavas. Hybrid (numerical-experimental) modeling of complex structures with linear and nonlinear components. *Nonlinear Dynamics*, 47(1-3):193–217, 2007.

[17] O.S. Bursi and D. Wagg, editors. *Modern Testing Techniques for Structural Systems*. Springer, Vienna, Austria, 2008.

[18] S. Yesilyurta and A. Patera. Surrogates for numerical simulations; optimization of eddy-promoter heat exchangers. *Computer Methods in Applied Mechanics and Engineering*, 121(1-4):231–257, 1995.

[19] F.A. Diazdelao, S. Adhikari, E.I. Saavedra Flores, and M.I. Friswell. Stochastic structural dynamic analysis using Bayesian emulators. *Computers & Structures*, 120:24–32, 2013.

[20] M.D. Spiridonakos and E.N. Chatzi. Metamodeling of dynamic nonlinear structural systems through polynomial chaos {NARX} models. *Computers & Structures*, 157:99 – 113, 2015.

[21] M.D. Spiridonakos and E.N Chatzi. Metamodeling of structural systems with parametric uncertainty subject to stochastic dynamic excitation. *Earthquakes and Structures/ An International Journal for Earthquake Engineering & Earthquake Effects on Structures*, 8(4):915–934, 2015. Special Issue on Structural Identification and Monitoring with Dynamic Data.

[22] M.D. Spiridonakos and S.D. Fassois. Adaptable functional series {TARMA} models for non-stationary signal representation and their application to mechanical random vibration modeling. *Signal Processing*, 96, Part A:63 – 79, 2014.

[23] C. de Boor. *A Practical Guide to Splines*. Springer-Verlag, Revised edition, 2001.

[24] M.D. Spiridonakos, V.K. Dertimanis, and E.N. Chatzi. Estimation of data-driven polynomial chaos using hybrid evolution strategies. In Y. Tsompanakis, J. Kruis, and B.H.V. Topping, editors, *Proceedings of the Fourth International Conference on Soft Computing Technology in Civil, Structural and Environmental Engineering*, Stirlingshire, UK, 2015. Civil-Comp Press. Paper 24.